Flow characteristics over a tractor-trailer model with and without vane-type vortex generator installed

Kin Hing Lo*, Konstantinos Kontis

Division of Aerospace Sciences, School of Engineering, University of Glasgow, University Avenue, Glasgow G12 8QQ, United Kingdom

ARTICLE INFO

ABSTRACT

An experimental study has been conducted to investigate the effects of vane-type vortex generators in affecting the flow pattern of the wake region using a 1:20 scale tractor-trailer model. The de Haviland wind tunnel of the University of Glasgow was employed in this study. Surface oil flow visualisation, smoke visualisation and two-component time-averaged particle image velocimetry measurements were used for flow diagnostics. Experimental data showed that putting the vortex generators near the front end of the trailer model could reduce the size of the vortex in the wake region. In addition, it was observed that the use of the vane-type vortex generators at the front of the trailer model might change the shear layer angle so that a smaller wake region was formed downstream of the trailer. No obvious effects of wake flow control could be observed by placing the vortex generators near the rear end of the trailer model. Finally, it was found that the vane-type vortex generator with the vane height of 6 mm is more effective in achieving wake flow control than the one with the vane height of 4 mm.

1. Introduction

Lorries play a major role in daily domestic freight transportation within the United Kingdom. According to the document "Transport Statistics Great Britain 2015" (Transport Statistics Great Britain, 2015), issued by the Department of Transport of the UK government, 73.5% of domestic freight was moved by lorries in 2014 (Transport Statistics Great Britain, 2015). In terms of emissions, in 2013, Heavy Goods Vehicles (HGVs) contribute 15.5 million tonnes or 13% of the total transport related greenhouse gas emissions in the United Kingdom (Transport Statistics Great Britain, 2015). Due to the fact that all HGVs have considerably blunt shapes, these vehicles encounter high level of aerodynamics drag during high speed operations. In fact, Bradley, (2000) concluded that about 21% of losses come from aerodynamics drag for a heavy vehicle weighting 36 t operating at 105 km/h. In other words, additional fuel is consumed in order to overcome the aerodynamic drag encountered by a heavy vehicle during high speed operations compared to the vehicle operating at low speed conditions. Altaf et al. (2014) stated that due to the poor aerodynamics efficiency of lorries and buses, up to 65% of fuel is consumed to overcome the aerodynamic drag encountered by these vehicles in long-haul journeys. It is anticipated that a significant amount of fuel could be saved by improving the aerodynamic efficiency of heavy vehicles (Bradley, 2000; Altaf et al., 2014). Quantitatively, (Bradley, (2000) found that about 4% of fuel saving could be achieved if the aerodynamic drag encountered by a heavy vehicle is reduced by 20% when operating at 105 km/h. Similarly, Hsu and Davis, (2010) stated that an annual fuel cost saving of about US$10,000 could be achieved for a 40% cut of the aerodynamic drag that acted on a heavy vehicle.

The aerodynamics characteristics of small-sized vehicles like cars and vans have been investigated extensively in the past two decades (Hucho and Sovran, 1993; Sovran et al., 1978). In contrast, the aerodynamic performance and geometry optimisation of heavy vehicles have received much less attention in both the academia and industrial sector. In fact, until now box-shaped heavy vehicles with sharp edges and corners around their bodies could still be seen frequently. This is partially due to the fact that aerodynamic performance is not a priority area of concern when designing heavy vehicles in most vehicle manufacturers' point of view. Instead, the primary goal that needs to be achieved in heavy vehicle designs is to minimise the space that is occupied by the engine, gearbox and other essential components of a vehicle so that the loading capacity could be maximised. This is particularly true for countries that have stringent regulations governing the maximum length, width and height of HGVs like most countries in Europe and some countries in Asia. Recently, this situation seems to change progressively due to the implementation of more stringent standards in terms of exhaust gas and noise emissions to Diesel-powered vehicles (i.e. most heavy vehicles) (European Commission

---

* Corresponding author.
E-mail addresses: kinhing.lo@glasgow.ac.uk (K.H. Lo), kostas.kontis@glasgow.ac.uk (K. Kontis).

transport emissions regulation webpage, 2016). In order to satisfy these stringent requirements, the aerodynamic efficiency of heavy vehicles needs to be taken into account. As a result, some heavy vehicle manufacturers recently starting to develop and introduce more aerodynamically efficient heavy vehicles into the market.

Amongst various types of HGVs, articulated lorries or tractor-trailers are one of the most common types of HGVs in the world. An articulated lorry is usually formed by joining a motorised tractor unit with a non-motorised trailer unit. As a result, many significant drag generation sources can be found on tractor-trailer vehicles although the majority of drag acting on these vehicles comes from four main areas known as the forebody stagnation region, the under-body flow, the tractor-trailer gap region and the flow separation at the rear end of the trailer. In fact, the drag contribution from these drag sources have been well documented in literatures (Cooper, 2003; Choi et al., 2014; Buil and Herrer, 2009; Wood and Bauer, 2003; Storms et al., 2001). In the past four decades, various flow control devices and strategies have been developed to achieve flow control in these four areas and their details are well documented and can be found in the review article recently published by Choi et al. (2014).

Since most of the trailers in articulated lorries are box-shaped and featured with sharp edges and corners, severe flow separation appears at the rear edge of a square back trailer. The occurrence of massive flow separation leads to the formation of a large wake region downstream of the rear end of the trailer (Altaf et al., 2014; Choi et al., 2014). As a result, significant amount of base drag is generated because the pressure within the wake region is low (Altaf et al., 2014; Hucho and Sovran, 1993). Wood, (2006) concluded that approximately 25% of aerodynamics drag encountered by a tractor-trailer vehicle is caused by the massive flow separation that appears at the rear end of the square back trailer. Due to this reasons, effective measures must be developed in order to reduce the amount of pressure drag that generated in this region. Surprisingly, until now, only a few devices have been developed in attempt to achieve drag reduction in the rear end of the square back trailers. These devices reduce the amount of base drag generated by either reducing the size of the wake region (e.g. vertical splitter plate (Gillieron and Kourta, 2010), flaps (Altaf et al., 2014), base cavities and boat tails (Balkanyi et al., 2002; Verzicco et al., 2002; Yi, 2007; Peterson, 1981; Croll et al., 1996) or by pushing the wake region away from the trailer (e.g. base bleeding (Gillieron and Kourta, 2010; Englar, 2001; Littlewood and Passmore, 2012; Howell et al., 2003)).

Amongst these devices, base bleeding has been proven to be an effective measure to achieve base drag reduction in tractor-trailer vehicles. In general, a minimum of 10% base drag reduction could be achieved using this flow control method (Gillieron and Kourta, 2010; Englar, 2001; Littlewood and Passmore, 2012; Howell et al., 2003). However, the presence of the heavy and bulky components in the jet blowing actuators limits the applicability of this flow control strategy in practice. In addition, although base drag reduction could be effectively achieved using base bleeding, a significant amount of power is consumed by the blowing pumps (Choi et al., 2014). Therefore, the amount of fuel that is saved from the base drag reduction by base bleeding is partially or completely outweighed by the additional fuel consumption for driving the blowing pump which further limits its applicability in actual practical situations (Balkanyi et al., 2002).

Other than base bleeding, the installation of the flaps (Altaf et al., 2014) or boat tails (Balkanyi et al., 2002; Verzicco et al., 2002; Yi, 2007; Peterson, 1981; Croll et al., 1996) could also effectively reduce the base drag by reducing the size of the wake region. Altaf et al. (2014) concluded that about 6−11% of base drag reduction could be achieved by installing trailing flaps with various lengths and shapes on to the rear end of a square back trailer. Similarly, Croll et al. (1996) found that up to 8% of base drag reduction could be achieved by a square back trailer equipped with a boat tail on to its rear end. Surprisingly, Yi, (2007) showed that potentially 42% of base drag reduction could be achieved in a square back trailer equipped with a boat tail with 15° slant angle. Although considerably promising results were obtained from these studies (Altaf et al., 2014; Yi, 2007; Croll et al., 1996), application of the trailing flaps or boat tails in achieving base drag reduction in actual tractor-trailer vehicles is uncommon because of the economical and operational constraints (Altaf et al., 2014; Choi et al., 2014). Moreover, in some countries that have tight regulations on the maximum allowable length of tractor-trailer vehicles, installation of the trailing flap or boat tail on to a trailer means that the trailer itself needs to be shortened so that the vehicle could be legally operated. This further limited the applicability of these devices in actual tractor-trailer vehicles.

Although base bleeding, boat tails and trailer flaps could effectively reduce the base drag generated, their applicability in practice is limited. Therefore, new economical and effective flow control devices that can be legally implemented in tractor-trailer vehicles in daily operation are still require to be developed (Choi et al., 2014). Surprisingly, one of the flow control devices called vortex generators that are commonly used in aircraft wings seems being overlooked in vehicle aerodynamic research. In fact, only a few studies (Leuschen and Cooper, 2006; Patten et al., 2012; Mugnaini, 2015) investigated the effects of vortex generators in achieving flow control in tractor-trailer vehicles. In the experimental study conducted by Leuschen and Cooper, (2006), the authors concluded that the fuel consumption and drag encountered by a full scale tractor-trailer vehicle with vortex generators installed around the rear end of the square back trailer was at least 1% higher than that encountered by the baseline vehicle. In contrast, previous study conducted by National Research Council Canada (Patten et al., 2012) and the numerical study conducted by Mugnaini, (2015) showed that less than 1% of fuel saving could be achieved in a tractor-trailer vehicle with vortex generators installed around the rear end of the trailer.

Although previous research (Leuschen and Cooper, 2006; Patten et al., 2012; Mugnaini, 2015) showed that installing vortex generators around the roof of the trailer could not significantly reduce drag encountered by the tractor-trailer vehicles, these studies did not investigate about how the vortex generators affected the flow pattern downstream of the rear end of a square back trailer. In addition, these studies (Leuschen and Cooper, 2006; Patten et al., 2012; Mugnaini, 2015) only investigated the flow control effects of vortex generators installed immediately upstream of the trailing edge of the trailer. It is unclear whether the flow pattern over a tractor-trailer vehicle could be altered by placing vortex generators to some more upstream locations. In fact, the results shown in (Correale, 2015) using a backward facing step concluded that vortex generators only provided positive effects when they are installed a distance upstream of the front edge of the backward facing step. This is because the function of vortex generators is to generate streamwise vortices that enhance mixing between the boundary layer and the freestream to increase momentum of the flow. This flow mixing process takes time and therefore, in order to obtain positive effects from this flow control method, the vortex generators should be installed a distance upstream of the location where flow separation begins.

The present experimental study aims to investigate the effects of vane-type vortex generators in affecting the flow pattern downstream of the rear end of a square back trailer using a 1:20 scale tractor-trailer model. In addition, the effects of the installation location of the vortex generators in affecting the flow pattern downstream of the rear end of a square back trailer are also investigated. The result obtained could improve our understanding about the effects of vane-type vortex generators in achieving flow control in tractor-trailer vehicles.

2. Experimental setup

2.1. Generic tractor-trailer model

A 1:20 scale generic tractor-trailer model was used in this experimental study. The geometry and dimensions of the model used is
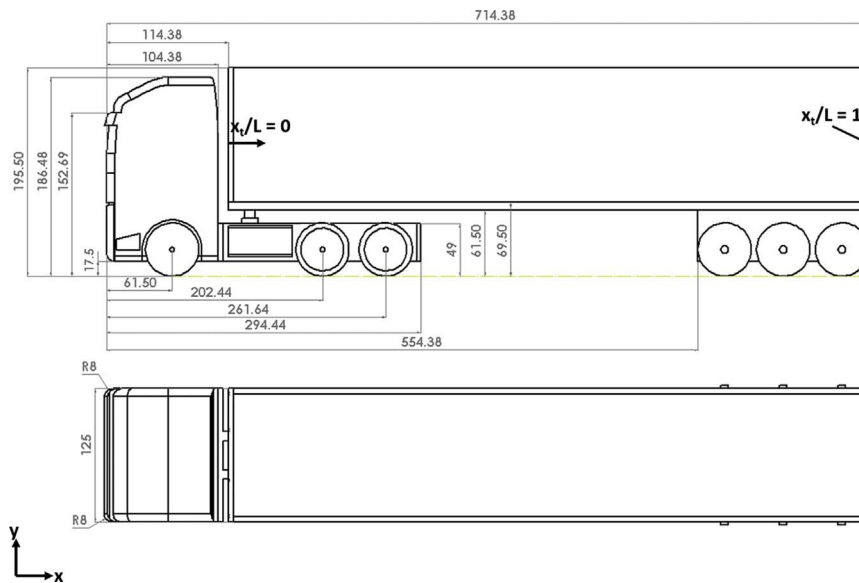
Fig. 1. Schematic of the 1:20 tractor-trailer model used.

shown in Fig. 1. The tractor model shape and dimensions were designed based on some actual articulated lorries that commonly found in the United Kingdom. The trailer model was designed based on the actual trailers manufactured by a trailer manufacturer in the United Kingdom. One key feature in the trailer model is that the axles and the wheels in the trailer model are supported by a hollow block instead of a solid block in order to simulate the wheel mounting method in actual trailers.

It should be noted that similar scale models were also employed by Taubert and Wygnanshi, (2007) and Ortega et al. (2007). The authors in (Taubert and Wygnanshi, 2007; Ortega et al., 2007) concluded that the flow features and drag values obtained using tractor-trailer models with this scale are comparable to that encountered by the actual vehicles. Similar conclusion was also drawn by Choi et al. (2014).

In order to simulate the operational conditions of the articulated lorries in motorways, the normalised gap size (i.e. the space between the tractor rear end and the front face of the trailer, $\sqrt{G/A}$) employed in this study was kept to minimal at $\sqrt{G/A}$ =0.1. It should be noted that G and A are the gap length (i.e. the length between the tractor rear end and the front face of the trailer) and the frontal area of the tractor model, respectively. Nineteen removable slots are provided at the front and rear ends of the trailer's roof so that the vortex generators could be installed at different locations along the roof of the trailer. In this study, the vortex generators were installed at two normalised locations (x_t/L) known as x_t/L=0.05 and 0.95 where L is the length of the trailer model which is 600 mm. It should be noted that x_t starts at the beginning of the trailer model at which x_t/L=0 and 1 are the front and rear end of the trailer model, respectively. It should be noted that other than the slot that occupied by the vortex generator, strips are inserted into all other unused slots to ensure that a flush surface of the trailer model is maintained.

2.2. Vane-typed vortex generators

Two counter-rotating oriented backward-facing vane-type vortex generators (VG) with different sizes (hereafter: VG1 and VG2) were used in the present study. Vane-type vortex generators were used because this type of vortex generators shows the highest effectiveness in achieving drag reduction in tractor-trailer vehicles as concluded by Mugnaini, (2015). A schematic of the vortex generator used is shown in Fig. 2. It should be noted that L, H and S shown in Fig. 2 are the length, height of the vanes and the separation distance between two vane pair, respectively.
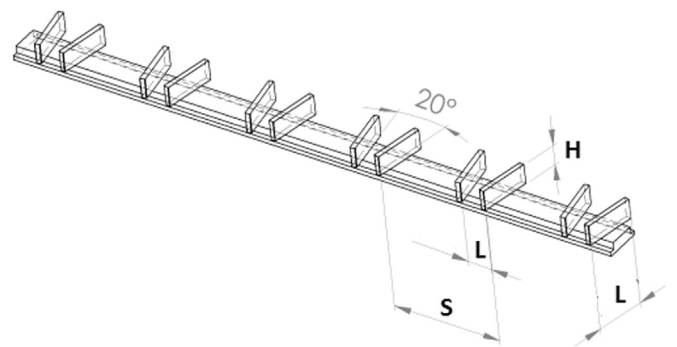

Fig. 2. Schematics of the vane-type vortex generators used.

The vane-type vortex generators were designed based on the boundary layer thickness (δ) predicted from an analytical study using a rectangular block with the dimensions same as the tractor-trailer model used in this study. The dimensions of the two vane-type vortex generators VG1 and VG2 are tabulated in Table 1.

2.3. Wind tunnel setup

Experiments were conducted using one of the low-speed wind tunnels at the University of Glasgow. A schematic of the experimental setup is shown in Fig. 3.

The wind tunnel has a closed-loop design and the contraction ratio between the settling chamber and the test section is 5:1. The wind tunnel test section has the dimensions of 4000 mm (length)x2700 mm (width)x2100 mm (height), Optical access to the wind tunnel test section is achieved through the two glass side windows and two ceiling mounted Perspex top windows. The freestream velocity was set to 50 ± 1 ms^{-1} and hence, the corresponding flow Reynolds number with respect to the height of the tractor model (Re$_H$) was Re$_H$=5.3×10^5. Although the flow Reynolds number is an order of magnitude lowered

Table 1
Dimensions of the two vane-type vortex generators, VG1 and VG2 used in this study.

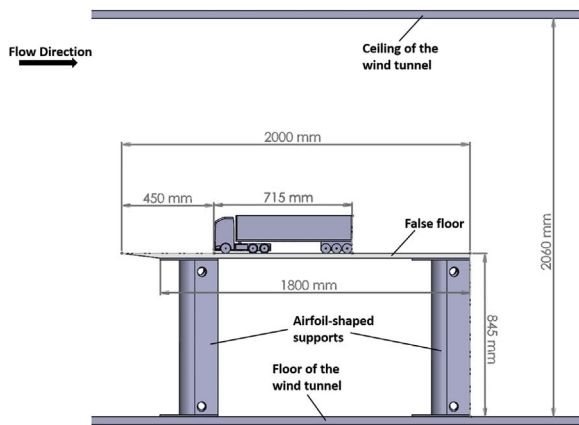|	Vane length, L (mm)	Vane height, H (mm)	Separation distance, S (mm)
VG1	10	4	44
VG2	15	6	66

Fig. 3. Schematic of the experimental setup of the tractor-trailer experiments.

than that encountered by actual tractor-trailer vehicles, Choi et al. (2014) noticed that the flow features that appear in the wake region of the models with this scale are comparable to those shown in actual vehicles. Under this freestream velocity, the freestream turbulent intensity level in the wind tunnel test section is about 0.4%.

The tractor-trailer model was mounted on a stationary false-floor situated in the wind tunnel test section. Similar experimental setup was also employed by Taubert and Wygnanshi, (2007) using a 1:24 scale tractor-trailer model. The length and width of the false-floor are 2000 mm and 800 mm, respectively. The false-floor was supported by two pairs of floor-mounted symmetrical airfoil-shaped supports and it was situated at 875 mm above the ground level of the wind tunnel. The tractor-trailer model was mounted at 450 mm downstream of the leading edge of the false-floor. The clean false floor was first calibrated using surface oil flow visualisation and Particle Image Velocimetry (PIV) measurement to ensure that the false floor is aligned with the freestream direction. Pitot measurements were conducted to measure the boundary layer thickness of the false floor (i.e. without mounting the model on it) at the location where the front of the tractor model is situated. The measured boundary layer thickness based on 99% freestream velocity is δ_{99}=10.7 mm and the corresponding displacement thickness is δ^*=1.18 mm. In addition, smoke visualisation was used to investigate the size of the spanwise vortices generated at the two sides of the false floor to ensure that these vortices do not induce any effects in affecting the flow pattern over the tractor-trailer model during the wind tunnel tests.

3. Flow diagnostics

3.1. Smoke oil visualisation

Qualitative streamwise flow pattern along the tractor-trailer model was examined using smoke visualisation technique. A Pea Soup SGS-90 smoke machine was used to generate the smoke used in the experiments. The smoke probe was precisely aligned to ensure that the smoke was delivered along the centreline of the tractor-trailer model. The smoke oil used was also supplied by Pea Soup (Model 135 Type A). The delivery rate and the voltage of the smoke machine were set to 80 mL per hour and 25 V, respectively. Illumination to the tractor-trailer model was provided by four 120 W white colour Light Emitting Diode (LED) flood lamps. These LED flood lamps were mounted on the ceiling along the centreline of the wind tunnel test section. The streamwise flow pattern along the tractor-trailer model was captured by a Photron FastCam SA1.1 monochrome high-speed camera situated at the port-side of the wind tunnel test section. The frame rate of the camera was set to 5000 frames per second in order to capture the unsteady effects in the flow field. The images captured were stored in a Windows-based personal computer.

3.2. Two-component particle image velocimetry measurements

Two-component Particle Image Velocimetry (PIV) measurements were conducted to obtain qualitative and quantitative time-averaged velocity and vorticity information along the centreline of the tractor-trailer model. A pair of Litron LPY742-100, Nd: YAG Q-switched lasers was used to provide illumination in the PIV measurements. These lasers have pulse energy of 100 mJ at a repetition rate of 200 Hz. The laser pulses have the wavelength and pulse width of 532 nm and 5 ns, respectively. The separation time between the laser pulses generated by the two lasers (Δt) was set to 10 μs so that sufficient displacement of the tracer particles could be achieved with the freestream velocity (U_∞) employed in the present study (i.e. U_∞=50 ms^{-1}). The time-averaged vector field of each test was constructed by averaging at least 2000 pairs of images. The laser beams generated by the two lasers were delivered to the ceiling of the wind tunnel test section through a series of flat mirrors. The laser beams were then expanded to a 2 mm thick laser sheet and illuminated along the centreline of the false floor. Olive oil particles with typical diameter of 1 μm were used as the seeder. The seeder particles were generated by a PIV Tech aerosol generator with the particle generation rate set to 10^8 particles per second. This setting ensured sufficient seeding was provided to the wind tunnel test section during the PIV measurements.

A Phantom v341 high-speed camera was used to record scattered light from the particles. A Sigma 105 mm fixed lens was attached to the camera with the aperture size set to F2.8. Through this arrangement the resolution of the camera was equal to 2560 pixelsx1600 pixels corresponding to the viewing area of 466 mm (length) x 291 mm (height). The captured images were stored in a Windows-based workstation and processed via the cross-correlation algorithm using the software Davis 8. The recorded image pairs were initially divided into a number of 32 pixelsx32 pixels interrogation windows and two passes of cross-correlation were conducted. The interrogation windows were then refined to 16 pixelsx16 pixels and another three passes of cross-correlation were conducted. A 50% overlap was employed in order to improve spatial resolution and to prevent the appearance of spurious vectors by adaptively improving the window size (Lo, 2014; Lo et al. 2016). Processed data were stored in a Windows-based personal computer and post-processed using the software Tecplot 360. Uncertainty of the PIV measurements were calculated using the method described in Lusk et al. (2012). It should be noted that similar method was also employed by Lo et al. 2016. Since at least 4000 individual images were used to construct the time-averaged vector field, the corresponding uncertainty of the PIV measurements in resolving the time-averaged vectors was about 3.75%.

4. Results and discussion

The time-averaged streamwise flow pattern along the centreline of the tractor-trailer model with and without vortex generator installed obtained from smoke visualisation is shown in Fig. 4.

From Fig. 4(a) to (e), it can be seen that the general streamwise flow pattern over the tractor-trailer model is similar in all five cases being studied and can be summarised as follows. Qualitatively, when the incoming flow reaches the front of the tractor model, part of the flow is halted by this front face of the model. As a result, a flow stagnation region appears on the front surface of the tractor model that can be clearly seen in Fig. 4(a) to (e). The incoming flow above the stagnation point turns upwards and reaches the top of the tractor model. After turning upwards, the flow reaches and expands along the curvature of the roof of the tractor model. The flow then reaches the rear end of the tractor and some of the flow enters the gap region between the tractor and the trailer whilst the rest of it crosses the gap and impinges over the front surface of the trailer model (i.e. the vertical line no. 1 shown in Fig. 4). Although the front edge of the trailer model is sharp, no obvious separation bubble could be observed immediately downstream
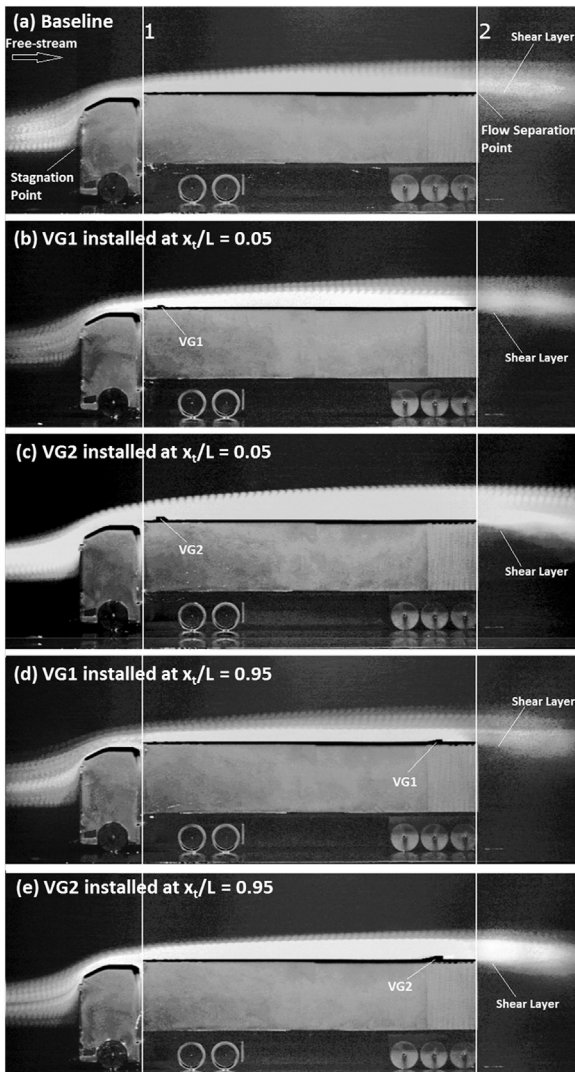
Fig. 4. Smoke visualisation images of the tractor-trailer model with and without vortex generator installed. (a) Baseline configuration (i.e. no VG installed), (b) VG1 installed at $x_t/L=0.05$, (c) VG2 installed at $x_t/L=0.05$, (d) VG1 installed at $x_t/L=0.95$ and (e) VG2 installed at $x_t/L=0.95$.

Fig. 5. Definitions of the thicknesses and angles that measured from the smoke visualisation images.

Table 2
Averaged thicknesses and angles of the smoke streaks measured using smoke visualisation images. Legends: Case A = Baseline model, Case B = VG1 installed at $x_t/L=0.05$, Case C=VG2 installed at $x_t/L=0.05$, Case D=VG1 installed at $x_t/L=0.95$ and Case E=VG2 installed at $x_t/L=0.95$.

Case	L.T. (mm)	T.T. (mm)	L1 (deg)	T1 (deg)	T2 (deg)
A	31.6 ± 2.1	58.6 ± 3.8	84.6 ± 1.0	91.1 ± 0.8	97.9 ± 3.0
B	31.5 ± 3.5	53.8 ± 3.8	84.4 ± 1.0	90.7 ± 0.8	104.0 ± 2.5
C	30.8 ± 3.1	53.1 ± 3.2	84.1 ± 1.6	91.1 ± 0.9	104.8 ± 2.2
D	31.7 ± 2.9	55.8 ± 3.3	84.2 ± 1.1	91.3 ± 0.8	99.7 ± 2.8
E	31.0 ± 3.1	55.7 ± 2.5	84.0 ± 1.1	91.4 ± 0.8	99.5 ± 2.3

shown in Fig. 5 to illustrate the locations where the angle and thickness measurements were taken. The results obtained from the measurements are tabulated in Table 2. It should be noted that the results shown in Table 2 were calculated by averaging the measurement results from 1000 instantaneous images captured from the smoke visualisation experiments. Once again, it must be emphasised that the data presented in Table 2 should be treated qualitatively as considerably amount of uncertainty could be arise by measuring thicknesses and angles directly from the images captured from the smoke visualisation experiments.

From Table 2, it can be seen that at the front section of the trailer model, the smoke streaks in all cases being studied show similar smoke streak thickness (L.T.) and shear layer angle (L1) regardless whether vortex generator is installed. This implies that the presence of the vane-type vortex generators at the front section of the trailer model as in Cases B and C does not induce any obvious flow tripping effects at the front region of the trailer. In contrast, compared to the baseline case (i.e. Case A), the presence of the vortex generators (i.e. Cases B to E) on the roof of the trailer model affects the properties of the smoke streaks at the rear end of the trailer model. This can be revealed by observing the data shown in Table 2 for the smoke streak thickness at the trailing edge T.T. and the upper and lower shear layer angles T1 and T2, respectively. From Table 2, it is clear that the smoke streak at the trailing edge of the trailer has the highest thickness in the baseline model (Case A, Fig. 4(a)). In contrast, compared to the baseline configuration, thinner smoke streak thicknesses T.T. are shown in those cases with the vane-type vortex generators installed on the roof of the trailer model (i.e. Case B to E, Fig. 4(b)–(e)). In general, the thickness of the smoke streak decreases with increasing the size of the vortex generators as the magnitudes of T.T. in those cases with the VG2 installed (i.e. Cases C and E) are always slightly smaller than those with the VG1 installed (i.e. Cases B and D). Moreover, the smoke streak thickness T.T. in those cases with the vortex generators installed at the front of the trailer (i.e. $x_t/L=0.05$, Cases B and C) are always slightly thinner than those cases when the vortex generators are presented at the rear (i.e. $x_t/L=0.95$, Cases D and E).

It is believed that the presence of the vane-type vortex generators on the roof of the trailer model induced interactions between the boundary layer and the freestream, thus changing the thickness of the smoke streaks at the trailing edge of the trailer model. In addition, the effect of smoke streak thinning seems to be more prominent in Cases B

of the front edge of the trailer model in all cases being studied. The boundary layer becomes progressively thicker along the trailer model which is evidenced by the gradually increasing thickness of the smoke streaks along the trailer in all cases being studied. Flow separation begins at the sharp rear edge of the trailer model (i.e. the location where the vertical line no. 2 is presented) in all cases being studied. As a result, fully separated flow appears downstream of the rear end of the trailer model.

Although the flow pattern over the tractor-trailer model seems usual as it is agreed with the general flow pattern concluded by Choi et al. (2014), it is worth to note an interesting observation from Fig. 4 here. Qualitatively, the shear layer seems to point the most downwards in the case when the vane-type vortex generator VG2 is installed at the normalised location $x_t/L=0.05$ (Fig. 4(e)) compared to other cases being studied as shown in Fig. 4(a)–(d). However, it must be emphasised that this is a qualitative observation only as the shading of the incident smoke, possibly caused by slightly non-constant emission rate of the smoke source, could affect the result that obtained from the smoke visualisation experiment.

In order to study the effects of the vortex generators in affecting the shear layer angle, the thicknesses and angles of the smoke streaks at various locations along the trailer model were measured. A schematic is
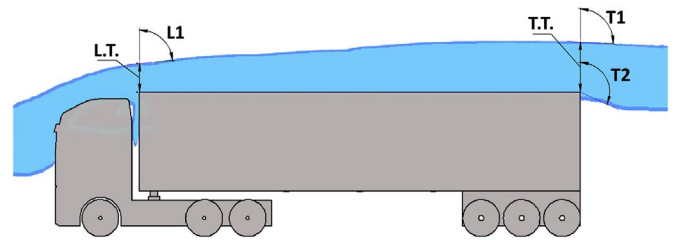
and C with the VG1 and VG2 installed at the normalised location $x_t/L=0.05$ than in cases D and E with the vortex generators installed at $x_t/L=0.95$. This is deduced that when the vortex generators are installed at the normalised location $x_t/L=0.05$, it is located far upstream of the trailing edge of the trailer and therefore, a longer distance is available for the vortex generators to induced flow mixing between the boundary layer and the freestream. As a result, a thinner smoke streak is formed at the trailing edge of the trailer model.

Other than the smoke streak thickness, another interesting phenomenon can be observed from the results that shown in Table 2 is the variation of the shear layer angle T2 in different trailer model configurations. From Table 2, it is clearly that the smallest shear layer angle appears in Case A (i.e. baseline case) while the largest shear layer angle appears in Case C with the vane-type vortex generator VG2 is installed at the normalised location $x_t/L=0.05$. A larger shear layer angle T2 in Table 2 means that the shear layer points more downwards relative to the freestream direction. Therefore, the shear layer points the most downwards in Case C (i.e. VG2 installed at $x_t/L=0.05$) while the least downwards in the baseline case (i.e. Case A). This finding implies that the re-circulation zone that appears behind the rear end of the trailer with the vortex generator VG2 installed at the front of the trailer is probably smaller than that appears in the baseline tractor-trailer configuration.

In addition, three additional trends could be observed from the results that presented in Table 2. The first trend that can be observed is that the shear layer angle in the trailer model with the vortex generators installed is always larger (i.e. pointing more downwards) than that shown in the baseline trailer (Case A). This can be revealed from Table 2 that the shear layer angle T2 in cases B to D are all larger (i.e. the shear layer points more downwards) than that shown in the baseline trailer (i.e. Case A). This finding implies that the use of the vane-type vortex generators on the roof of the trailer model could provide positive effects in reducing the size of the wake region downstream of the trailer rear end. Moreover, amongst those cases with vane-type vortex generators installed on the trailer roof (i.e. Cases B to D), it was found that the shear layer angle is always larger when the vane-type vortex generators are installed near the front end (i.e. Cases B and C) than they are installed near the rear end (i.e. Cases D and E) of the trailer. In fact, from Table 2, it can be seen that the shear layer angle T2 for the case when the vortex generator VG1 is installed at the normalised location $x_t/L=0.05$ (i.e. Case B) is larger than that when it is installed at the normalised location $x_t/L=0.95$ (i.e. Case D). Similar trend also observed when the bigger vane-type vortex generator VG2 is used (i.e. Cases C and E). This finding indicated that the wake region that formed behind the rear end of the trailer model may be smaller when the vortex generators are installed at the front of the trailer. Finally from Table 2, it can be observed that for a given vortex generator installation location, both vane-type vortex generators VG1 and VG2 produce similar effect in changing the shear layer angle. To be exact, for a given normalised position, the shear layer angle remains similar regardless which vane-type vortex generator VG1 or VG2 is installed on the roof of the trailer model.

In fact, the findings from Table 2 can be further investigated by studying the flow streamlines in the wake region obtained from the time-average PIV measurements as shown in Fig. 6. It should be noted that normalised coordinates x/H and y/H are used in Fig. 6 where H is the height of the trailer model which is 125 mm. In addition, the background contour in Fig. 6 represents the normalised velocity magnitude of the flow field. Qualitatively, from Fig. 6(a) to (e), it can be seen that the flow pattern in the wake region behind the rear end of the trailer model remains considerably similar in all cases being studied. In general, a large recirculating flow region is formed immediately downstream of the rear end of the trailer model. In addition, reverse flow and three-dimensional flow structures are observed immediately downstream of the recirculating flow region (i.e. in the region between $0 < x/H < 1.2$ and $-0.4 < y/H < 0.8$). The

flow in and immediately downstream of the recirculating flow region has relatively low velocity compared to the freestream. In fact, similar wake flow pattern also documented in (Mugnaini, 2015; Hucho, 1998; Fujimoto et al., 1992; Lajos and Hegel, 1994) using various square back heavy vehicle models.

In order to obtain information about the effects of the vane-type vortex generators in affecting the size of the recirculating flow region downstream of the trailer model, an additional batch of smoke visualisation experiments were conducted to visualise the actual flow pattern in the wake region of the trailer model. The result obtained is shown in Fig. 7. From Fig. 7(a) to (e), it can be seen that the flow pattern shown in the wake region obtained through smoke visualisation is similar to that obtained through PIV measurements (Fig. 6(a) to (e)). The size of the recirculation flow region in each case can be obtained by measuring various lengths of the vortex that formed in the wake region. Totally three lengths, known as the Outer Core Diameter (OCD), the Inner Core Diameter (ICD) and the Vortex Core Diameter (VCD), were measured and averaged using 1000 instantaneous smoke visualisation images. The schematic in Fig. 8 shows the definition of the lengths OCD, ICD and VCD used in the measurements and the results obtained from the measurements are tabulated in Table 3.

It can be seen from Table 3 that amongst all cases being studied, the size of the wake vortex in the baseline trailer configuration is the biggest. In fact it can be revealed by observing Fig. 7(a) –(e) that the largest vortex appears in the wake region of the baseline trailer (i.e. case (a)). In contrast, from Table 3, it can be seen that the wake vortex that formed behind the rear end of the trailer has smaller sizes in those trailers with the vane-type vortex generators installed on the roof (i.e. cases (b)–(e)). In addition, from both Fig. 7(a) to (e) and the data shown in Table 3, it can be seen that when the vortex generators are installed near the front end of the trailer model (i.e. $x_t/L=0.05$) the corresponding wake vortex that formed is smaller than when they are installed near the rear end of the trailer (i.e. $x_t/L=0.95$). This phenomenon occurs in both the VG1 and VG2 used in the present study. These results obtained further suggest that the vane-type vortex generators installed near the front on the trailer roof may be able to reduce the extent of flow separation that appears downstream of the rear end of the trailer. Moreover, it can be seen from Table 3 that the size of the wake vortex is smaller when the larger vortex generator VG2 is used (i.e. cases (c) and (e)) compared to that when the smaller vortex generator VG1 is used (i.e. cases (b) and (d)).

In fact, by comparing the size of the wake vortex between the case when the VG2 is installed at the normalised location $x_t/L=0.05$ (i.e. case (c)) and the baseline case (i.e. case (a)), it can be seen that the outer diameter of the wake vortex (OCD) in case (c) is about 12.9% smaller than that shown in the baseline case (case (a)). A similar trend also appears when the smaller vane-type vortex generator VG1 is installed at the normalised location $x_t/L=0.05$ of the trailer model (case (b)). With this configuration, the outer diameter of the wake vortex (OCD) is around 10.7% smaller than that shown in the baseline trailer. The results obtained indicate that the size of the recirculating flow region that formed immediately downstream of the rear end of a square back trailer could be reduced by installing counter-rotating oriented backward-facing vane-type vortex generators at the front of the square-back trailer. As already mentioned in previous subsections, this is deduced to be caused by the reason that longer time is available for the vortex generators to induce flow mixing between the freestream and the boundary layer when the vortex generator is installed near the front end of the trailer model. As a result, the flow that reached the rear end of the trailer has higher momentum and hence, the resulting level of flow separation is reduced.

In contrast, no significant differences in terms of the wake vortex size can be observed in those cases when the vane-type vortex generators are installed near the rear end of the trailer model (i.e. case (d) and (e)) compared to the baseline case (i.e. case (a)). In fact, it can be calculated using the data shown in Table 3 that by installing
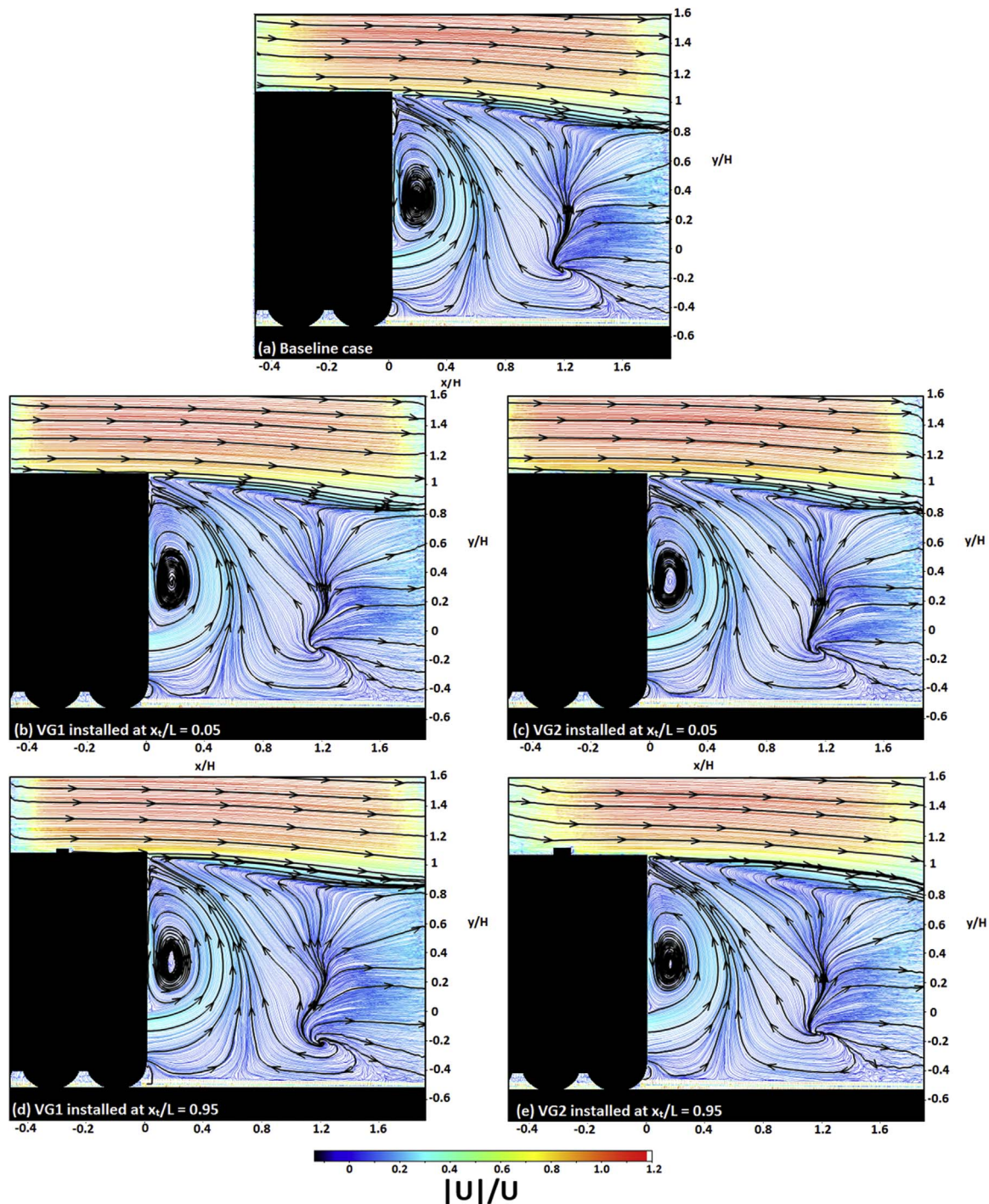
Fig. 6. Flow streamlines along the wake region of the trailer model with and without vane-type vortex generators installed. (a) Baseline model, (b) VG1 installed at $x_t/L=0.05$, (c) VG2 installed at $x_t/L=0.05$, (d) VG1 installed at $x_t/L=0.95$ and (e) VG2 installed at $x_t/L=0.95$.

VG1 (i.e. case (d)) and VG2 (i.e. case (e)) at the normalised location $x_t/L=0.95$, the outer diameter of the wake vortex (OCD) is only 2.8% and 5.8% smaller than that shown in the baseline trailer, respectively. This is because when the vortex generator is installed near the rear end of the trailer model, the distance and time available for the vortex generator to induce flow mixing become limited before reaching the trailing edge of the trailer. As a result, the momentum of the flow that reached the trailing edge of the trailer in these cases remains similar to that of the baseline trailer. As a result, similar extent of flow separation appears downstream of the rear end of the square back trailer.

Other than the size of the recirculating flow region, the flow velocity in the wake region is also an important parameter to justify the effects

of the vane-type vortex generators in achieving flow separation control on square back tractor-trailer vehicles. The normalised x- and y-velocity contours captured along the wake region of the trailer model are displayed in Fig. 9 (left) and (right), respectively.

From Fig. 9 (left), it can be seen that the x-velocity contour is quite similar in all cases being studied. Qualitatively, the presence of the vane-type vortex generators on the roof of the trailer does not induce any observable changes in the flow velocity in x-direction along the wake region. In contrast, the normalised y-velocity contours shown in Fig. 9 (right) indicate that the vane-type vortex generators on the roof might exert effects in changing the flow characteristics in y-direction. Qualitatively, from Fig. 9 (right), it can be seen that the baseline trailer
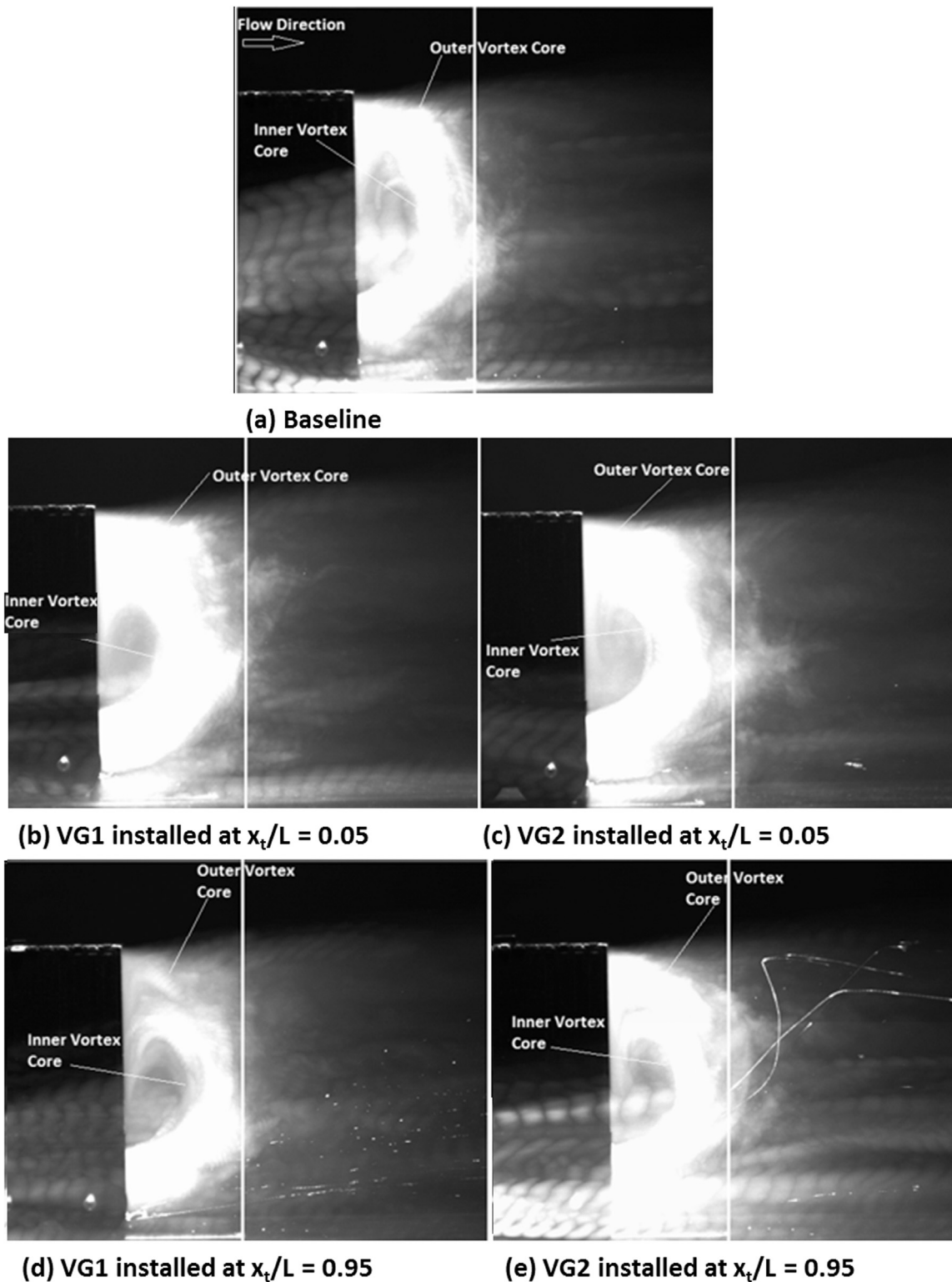
Fig. 7. Flow pattern of the recirculating flow region downstream of the rear end of the trailer model with and without VG installed. (a) Baseline model, (b) VG1 installed at x_t/L=0.05, (c) VG2 installed at x_t/L=0.05, (d) VG1 installed at x_t/L=0.95 and (e) VG2 installed at x_t/L=0.95.

(Fig. 9 [right] (a)) has the largest region that shows strong normalised y-velocity in the region between $0.3 < x/H < 0.6$. In contrast, for those cases with the vortex generators installed on the roof of the trailer (Fig. 9 [right] (b–e)), the region that shows strong normalised y-velocity is considerably smaller. Quantitatively, the flow characteristic along the wake region downstream of the rear end of the trailer can be investigated by plotting the normalised x- and y-velocity profiles at

various normalised locations (x/H) along the wake region. It should be noted that H is the height of the trailer model which is 125 mm. The resulting x- and y-velocity profiles plotted at the normalised locations x/H=0.2, 0.5 and 0.8 are shown in Figs. 10 and 11, respectively.

It is clear that some phenomena can be observed from Fig. 10 (a) to (c). Firstly, in the wake region between $0.3 < y/H < 1$ downstream of the trailer model, the normalised x-velocity shown in the baseline
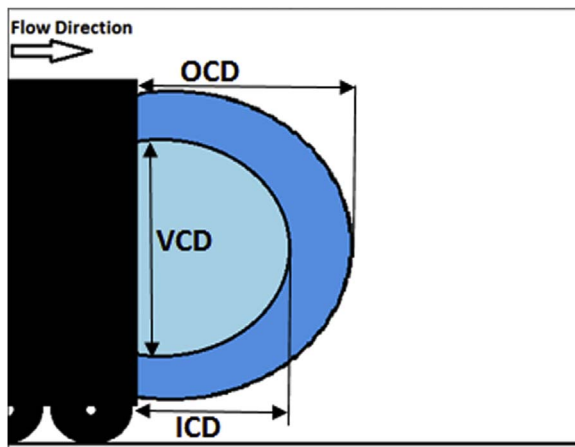
Fig. 8. Definitions of various lengths measured and averaged from 1000 instantaneous smoke visualisation images.

Table 3
Data of the main vortex measured from the wake region behind the trailer model.

Case	OCD (mm)	ICD (mm)	VCD (mm)
(a) Baseline (i.e. No VG)	94.2 ± 5.2	60.4 ± 2.3	51.9 ± 3.5
(b) VG1 installed at $x_t/L=0.05$	84.1 ± 6.1	52.5 ± 3.3	43.8 ± 3.9
(c) VG2 installed at $x_t/L=0.05$	82.1 ± 6.6	48.7 ± 3.0	40.7 ± 3.9
(d) VG1 installed at $x_t/L=0.95$	91.5 ± 5.1	58.5 ± 3.1	50.4 ± 4.0
(e) VG2 installed at $x_t/L=0.95$	88.7 ± 4.8	53.2 ± 3.3	43.4 ± 3.3

trailer is always the lowest (i.e. the most negative) in all the three normalised locations being studied. This indicated that strongest reverse flow appears in the wake region of the baseline trailer. In addition, from Fig. 10 (b), it can be observed that the lowest x-velocity appears around x/H=0.5 and y/H=0.6 in the wake region of the baseline trailer. The second strongest reverse flow appears at the same normalised x-location in the case when the smaller vane-type vortex generator VG1 is installed at the rear of the trailer (i.e. $x_t/L=0.95$). In this case, the reverse flow in the wake region is slightly weaker (i.e. slightly higher x-velocity) than that shown in the baseline trailer. The lowest x-velocity in this case appears in the region between 0.5 < y/H < 0.8. In addition, compared to the baseline case, it can be seen that the x-velocity over the entire wake region is higher (i.e. less negative) when the vane-type vortex generator VG1 is installed at the rear of the trailer model. The result obtained implies that the structure of the wake region was altered by the presence of the vane-type vortex generators on the roof of the trailer model. The presence of the vortex generators seems to weaken the wake vortex that formed behind the rear end of the trailer. Similar normalised x-velocity profiles are shown in both x/H=0.2, 0.5 and 0.8 in the trailer model with VG1 installed at x/H=0.05 and both VG1 and VG2 installed at x/H=0.95 as shown in Fig. 10 (a) to (c). Compared to the baseline case, the normalised x-velocity over the entire wake region in these three cases being studied is considerably higher than that appeared in the baseline case. This further suggests that the use of the vane-type vortex generators on the roof of the trailer might be able to weaken the recirculating flow in the wake region.

In contrast, from Fig. 11 (a), at the location x/H=0.2, similar normalised y-velocity profiles are shown in all cases being studied. This implies that the vortex generators on the roof of the trailer model seems to exert no obvious effects in changing the flow characteristics in y-direction at that normalised x-location. Downstream of x/H=0.2, it can be seen that at the normalised locations x/H=0.5 (Fig. 11 (b)) and x/H=0.8 (Fig. 11 (c)), the baseline trailer shows the highest positive normalised y-velocity in the region between −0.2 < y/H < 0.6. Lower levels of normalised y-velocity could be observed at all the three normalised x-locations along the wake region being studied for all

the trailers with the vane-type vortex generators installed on the roof. These results further suggest that the recirculating flow that presents in the wake region of the baseline trailer is the strongest amongst all other cases with vane-type vortex generators installed on the roof of the trailer being studied.

Fig. 12 displays the normalised z-vorticity profiles measured along the wake region of the trailer model. From Fig. 12 (a), it is clear that at the normalised x-location x/H=0.2, the strongest negative normalised z-vorticity appears between 0.9 < y/H < 1.1 (i.e. the upper shear layer) when the larger vane-type vortex generator VG2 is installed near the front of the trailer model. Similar trend also shown when the smaller vane-type vortex generator VG1 is installed near the near the front of the trailer model. However, similar normalised z-vorticity levels are shown in both the baseline trailer and those trailers with the vortex generators installed near the rear end on the roof. This finding suggests that installing the vane-type vortex generators near the front could increase the flow vorticity immediately downstream of the rear end of the trailer model. Further downstream along the wake region (i.e. x/H=0.5 and 0.8), from Fig. 12 (b) and (c), it can be seen that the normalised z-vorticity levels become similar in all cases being studied. This indicates that the effect in increasing flow vorticity provided by the vane-type vortex generators installed near the front of the trailer could only exert effects to a short distance in the wake region of the trailer model.

5. Limitations of the present study and future research recommendations

The present experimental study investigated the effects of vane-type vortex generators in achieving flow separation control in articulated lorries. However, there are three main limitations existed in this study and the details of these limitations and some future research suggestions are discussed in the following subsections.

5.1. Radius effect of the tractor front face

The tractor model used in the present study is a simplified 1:20 scale Volvo FH16 tractor unit. In order to ensure that the model has similar geometric features as shown in the actual vehicle, the geometry and dimensions of the model were directly scaled down from the actual vehicle. This means that the radius of the front corners in the tractor model (R_{front}) is considerably small (i.e. R_{front}=8 mm). Wood, (2012) suggests that the flow pattern over the front corners of a tractor model is highly sensitive to the flow Reynolds number. Since a 1:20 scale model is used in the present study, therefore the flow Reynolds number of the model is an order of magnitude smaller than that of the actual vehicle. This implies that the flow pattern over the two sides of the model could be different from that over the actual tractor vehicle. As the main objective of the present study is to investigate the streamwise flow pattern over a tractor-trailer model with vane-type vortex generators installed on the roof of the trailer, therefore, the front corner radius effects were not particularly considered in this study. However, it is recommended that the front corner radius should be corrected in order to account for the flow Reynolds number effects when designing scale tractor models for wind tunnel tests.

5.2. Plane of PIV measurement

The second main limitation that appears in the present experimental study is that currently only PIV data that measured along the centreline of the false floor could be provided. This is because the rail that used to mount the laser optics is situated along the centreline of the wind tunnel test section. Since the flow pattern over a tractor-trailer is fully three-dimensional, therefore, the effects induced by the vane-type vortex generators on the roof of the trailer model might be different if the data collected from other planes of measurements is also
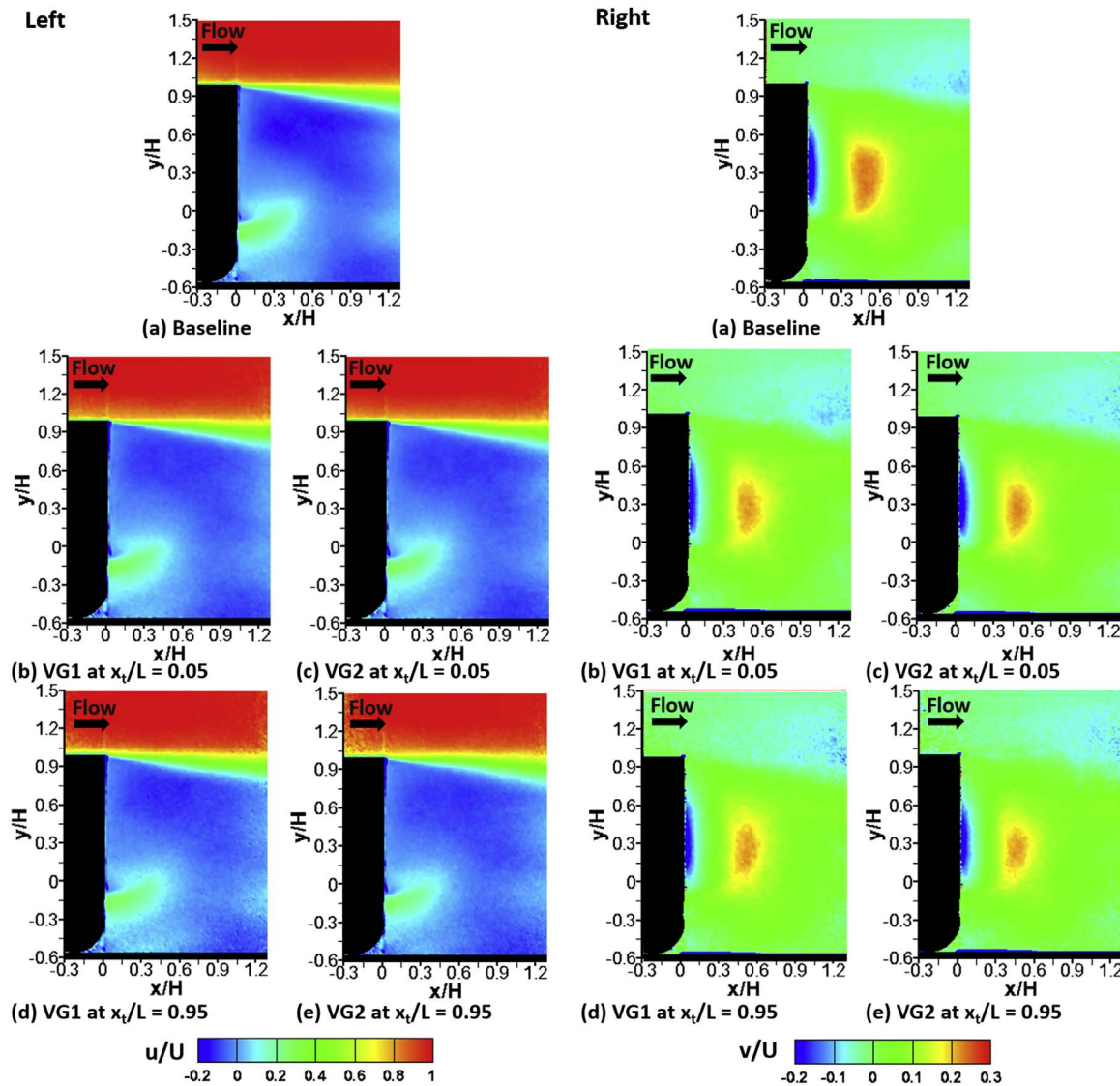
Fig. 9. The x- (left) and y- (right) velocity contours of the flow in the wake region of the trailer model with and without VG installed. (a) Baseline model, (b) VG1 installed at $x_t/L=0.05$, (c) VG2 installed at $x_t/L=0.05$, (d) VG1 installed at $x_t/L=0.95$ and (e) VG2 installed at $x_t/L=0.95$.

taken into account. Due to this reason, it is highly recommended that PIV measurements on other planes, in both streamwise and spanwise directions, should be conducted in order to fully resolve the flow physics along the wake region of the tractor-trailer vehicles.

5.3. Drag measurement

Another limitation of the present study is that the drag force that acting on the scale tractor-trailer model could not be measured from the wind tunnel test. This is due to the sting balance that installed in the wind tunnel is designed for measuring aerodynamic forces and moments of large-scale aircraft models. Since the size of the tractor-trailer model used in the present study is relatively small, the resolution of the sting balance is insufficient to accurately resolve the drag force that acting on the model due to its small size. In addition, the diameter of the sting is bigger than the size of the trailer model that used in the present study. This means that incorporating the sting into the trailer model is infeasible.

6. Conclusion

An experimental study has been conducted to investigate the effects

of the vane-type vortex generators in affecting the flow characteristics downstream of the rear end of a 1:20 square back tractor-trailer model. Two vane-type counter-rotating oriented and backward facing vortex generators with different height and separation distance, known as VG1 and VG2, were employed. Smoke visualisation and two-component particle image velocimetry measurements were used for flow diagnostics. The flow Reynolds number with respect to the height of the tractor model was 5×10^5 with the corresponding freestream velocity equal to 50 ms^{-1}.

Based on the images collected from the smoke visualisation experiments, it was observed that flow separation appeared immediately downstream of the rear end of the square back trailer model in all cases being studied. However, from the shear layer angle measurements, it was observed that the shear layer angle was the largest or points the most downwards in the case when the bigger vane-type vortex generator VG2 was installed at the normalised location $x_t/L=0.05$ on the roof of the trailer model. In addition, it was observed that compared to the baseline case, the presence of the vane-type vortex generators on the roof of the trailer could reduce the size of the recirculating flow region although this approach seems to be more effective when the larger vane-type vortex generator VG2 is used and the vortex generators are installed near the front end of the trailer
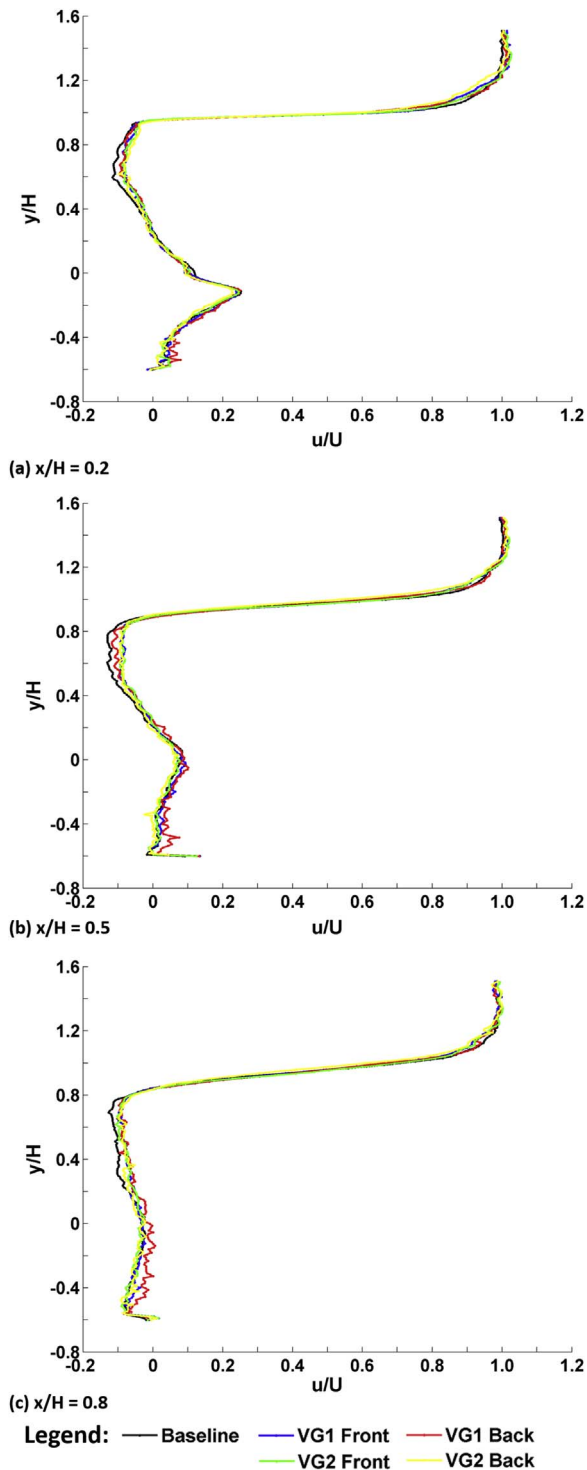
Fig. 10. Flow velocity profiles in x-direction in various normalised transverse location along the wake region of the trailer model with and without VG installed (a) $x_t/H=0.2$, (b) $x_t/H=0.5$ and (c) $x_t/H=0.8$.

Fig. 11. Flow velocity profiles in y-direction in various normalised transverse location along the wake region of the trailer model with and without VG installed (a) $x_t/H=0.2$, (b) $x_t/H=0.5$ and (c) $x_t/H=0.8$.

model. It is deduced that putting the vortex generators near the front end of the trailer model leads to longer time and distance available for the flow mixing between the freestream and the boundary layer to take place before flow separation begins. As a result the flow pattern downstream of the rear end of the trailer model is altered in this case.

In fact, the measurements of the size of the recirculating region that appeared immediately downstream of the square back trailer model showed that, compared to the baseline trailer, the size of the wake vortex was reduced by 10.7% and 12.9% when the vortex generators
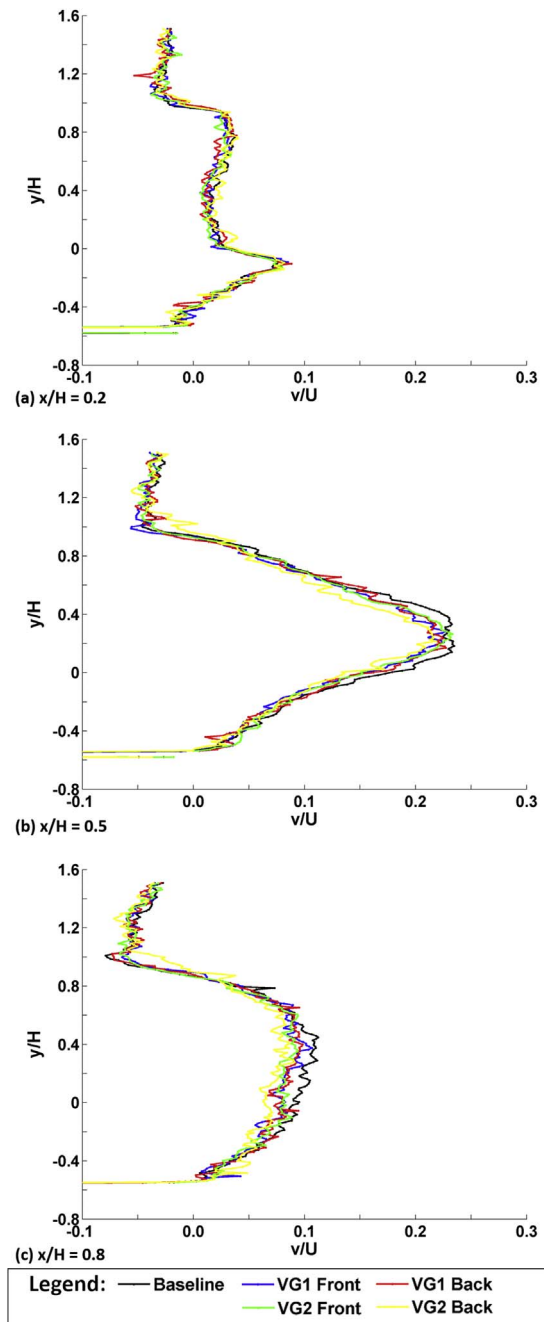
VG1 and VG2 were installed at the normalised location $x_t/L=0.05$, respectively. This implied that by installing the vane-type vortex generators near the front end of the trailer model might be able to effectively reduce the size of the wake region that formed downstream of the rear end of the trailer. In contrast, placing the vortex generators near the rear end of the trailer could only marginally reduce the size of the wake vortex by about 2.8% and 5.8% for the VG1 and VG2, respectively.

Finally, the x- and y-velocity profiles plotted at various normalised locations along the wake region of the trailer model showed that the strength of the reverse flow over the entire wake region is always the strongest in the baseline trailer. The use of the vane-type vortex generators on the roof of the trailer might be able to reduce the strength of the reverse flow that occurred in the wake region down-
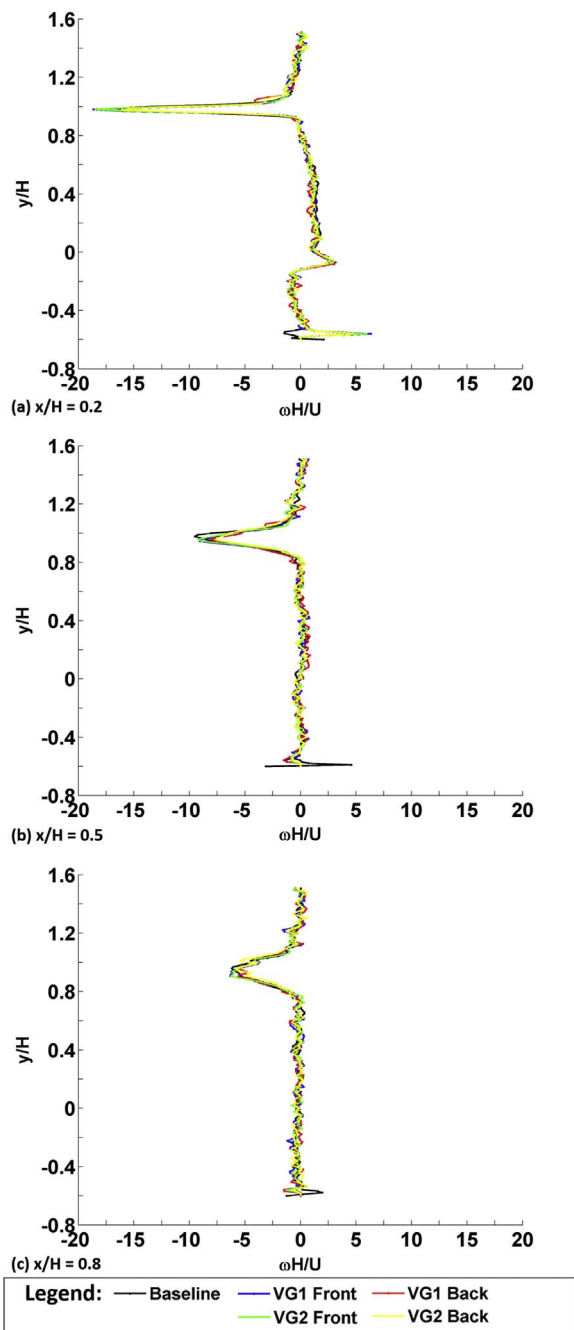
Fig. 12. Normalised z-vorticity profiles in various normalised transverse location along the wake region of the trailer model with and without VG installed (a) x_t/H=0.2, (b) x_t/H=0.5 and (c) x_t/H=0.8.

stream of the trailer. It was observed that using the bigger vane-type vortex generator VG2 as well as installing the vortex generators near the front end of the trailer model showed similar effects in reducing the strength of reverse flow over the wake region. Therefore, the results obtained from this experimental study suggest that the wake flow downstream of the rear end of a square back trailer might be potentially controlled by backward-facing vane-type counter-rotating oriented vortex generators installed on the roof of the trailer.

Author contributions

All experiments were conducted by Kin Hing Lo. Data analysis was conducted by Kin Hing Lo and Konstantinos Kontis. The manuscript was prepared and edited by both Kin Hing Lo and Konstantinos Kontis.

Conflicts of interest

The authors declare no conflict of interest.

Acknowledgments

References

Transport Statistics Great Britain, 2015. Department of Transport 2015. United Kingdom Government, United Kingdom.

Bradley, R., 2000. Technology Roadmap for the 21st Century Truck Program. Technical Report 21 CT-001, United States Department of Energy, Washington DC, United States.

Altaf, A., Omar, A.A., Asrar, W., 2014. Passive drag reduction of square back road vehicles. J. Wind Eng. Ind. Aerodyn. 134, 30–43.

Hsu, F.-H., Davis, R.L., 2010. Drag reduction of tractor-trailers using optimized add-on devices. J. Fluid Eng. 132, 0845041–0845046.

Hucho, W.-H., Sovran, G., 1993. Aerodynamics of road vehicles. Annu. Rev. Fluid Mech. 25, 485–537.

Sovran, G., Morel, T., Mason, W.T., Jr., 1978. Aerodynamic drag mechanism of bluff bodies and road vehicles 1st ed.. Springer, US, United States, 7–44.

European Commission Transport Emissions Regulation Webpage. ⟨http://ec.europa.eu/environment/air/transport/road.htm⟩ (Date of Visit: 12 October, 2016).

Cooper, K.R., 2003. Truck aerodynamics reborn-lessons from the past. SAE Tech. Pap., 2003-01-3376.

Choi, H., Lee, J., Park, H., 2014. Aerodynamics of heavy vehicles. Annu. Rev. Fluid Mech. 46, 441–468.

Buil, R.M., Herrer, L.C., 2009. Aerodynamic analysis of a vehicle tanker. J. Fluid Eng. 131, 0412041-004120417.

Wood, R.M., Bauer, X.S., 2003. Simple and low-cost aerodynamic drag reduction devices for tractor-trailer trucks. SAE Tech. Pap., 2003-01-3377.

Storms, B.L., Ross, J.C., Heineck, J.T., Walker, S.M., Driver, D.M., Zilliac, G.G., 2001. An experimental study of the ground transportation system (GTS) model in the NASA Ames 7- by 10-ft wind tunnel NASA/TM-2001-209621 Technical report of National Aeronautics and Space Administration, NASA, Washington, DC, United States.

Wood, R.M., 2006. A discussion of a heavy truck advanced aerodynamic trailer system. In: Proceedings of the 9th International Symposium on Heavy Vehicle Weights and Dimensions, Presented at the International Forum of Road Transport Technology (IFRTT); June 18–22 2006, Pennsylvania State University, State Colleague Pennsylvania, United States

Gillieron, P., Kourta, A., 2010. Aerodynamic drag reduction by vertical splitter plates. Exp. Fluids 48, 1–16.

Balkanyi, S.R., Bernal, L.P., Khalighi, B., 2002. Analysis of the near wake of bluff bodies in ground proximity. ASME Pap., 2002–32347.

Verzicco, R., Fatica, M., Iaccarino, G., Moin, P., Khalighi, B., 2002. Large eddy simulation of a road vehicle with drag-reduction devices. AIAA J. 40, 2447–2455.

Yi, W., 2007. Drag Reduction of a Three-Dimensional Car Model Using Passive Control Device (Ph.D. thesis). Seoul National University, Korea.

Peterson, R.L., 1981. Drag reduction obtained by the addition of a boattail to a box shaped vehicle.. Technical report of National Aeronautics and Space Administration NASA-CR-163113. NASA, Washington, DC, United States.

Croll, R.H., Gutierrez, W.T., Hassan, B., Suazo, J.E., Riggins, A.J., 1996. Experimental investigation of the ground transportation system (GTS) project for heavy vehicle drag reduction. SAE Tech.Pap., paper no. 960907.

Englar, R.J., 2001. Advanced aerodynamic devices to improve the performance, economics, handling and safety of heavy vehicles. SAE Tech. Pap., 2001-01-2072.

Littlewood, R.P., Passmore, M.A., 2012. Aerodynamic drag reduction of a simplified squareback vehicle using steady blowing. Exp. Fluids 53, 519–529.

Howell, J., Sheppard, A., Blakemore, A., 2003. Aerodynamic drag reduction for a simple bluff body using base bleed. SAE Tech. Pap., 2003-01-0995.

Leuschen, J., Cooper, K.R., 2006. Full-scale wind tunnel tests of production and prototype, second-generation aerodynamic drag-reducing devices for tractor-trailers. SAE Tech. Pap., 2006-01-3456.

Patten, J., McAuliffe, B., Mayda, W., Tanguay, B., 2012. Review of Aerodynamic Drag Reduction Devices for Heavy Trucks and BusesTechnical Report of National Research Council Canada. Center for Surface Transportation Technology, Ottawa, Canada, CSTT-HVC-TR-205.

Mugnaini, C.M., 2015. Aerodynamic Drag Reduction of a tractor-trailer using vortex generators: a computational fluid dynamic study (Master of Science thesis). California State University, Sacramento, United States.

Correale, G., 2015. Flow control over a backward facing step by ns-DBD plasma actuator. In: Proceedings of the 45th AIAA Fluid Dynamics Conference, AIAA Aviation, 22–26 June 1983. Dallas, TX, United States.

Taubert, L., Wygnanshi, I., 2007. Preliminary experiments applying active flow control to a 1/24th scale model of a semi-trailer truck. In: Proceedings of the International

Conference on Aerodynamics of Heavy Vehicles II: Trucks, Buses and Trains, 26–31 August 2007. Lake Tahoe, California, United States.

Ortega, J., Salari, K., Storms, B., 2007. Investigation of tractor base bleeding for heavy vehicle aerodynamic drag reduction. In: Proceedings of the International Conference on Aerodynamics of Heavy Vehicles II: Trucks, Buses and Trains, 26–31 August 2007. Lake Tahoe, California, United States.

Lo, K.H., 2014. Experimental Studies on Contour Bumps and Cavities at Supersonic Speed. (Ph.D. thesis). University of Manchester, Manchester, United Kingdom.

Lo, K.H., Zare-Behtash, H., Kontis, K., 2016. Control of Flow Separation on a Contour Bump by Jets in a Mach 1.9 Freestream: an Experimental Study. *Acta Astronautica* 126, 229–242.

Lusk, T., Cattafesta, L., Ukeiley, L., 2012. Leading edge slot blowing on an open cavity in supersonic flow. Exp. Fluid 53, 187–199.

Hucho, W.-H., 1998. Commercial vehicles. In: Aerodynamics of Road Vehicles4th ed.. SAE International, Warrendale, PA, United States, 473.

Fujimoto, T., Miyake, N., Watanabe, Y., Takeyama, T., 1992. Suppression of mud adhesion to the rear surface of a van-type truck. SAE Tech. Pap., 920203.

Lajos, T., Hegel, I., 1994. Some experiments of ground simulation with moving belt. In: Proceedings of the Vehicle Aerodynamics Conference, 18–19 July 1994. Loughborough, United Kingdom.

Wood, R., 2012. A review of reynolds number effects on the aerodynamics of commercial ground vehicles. SAE Int. J. Commer. Veh. 5, 628–639.